

Copyright © 1990, by the author(s).  
All rights reserved.

Permission to make digital or hard copies of all or part of this work for personal or classroom use is granted without fee provided that copies are not made or distributed for profit or commercial advantage and that copies bear this notice and the full citation on the first page. To copy otherwise, to republish, to post on servers or to redistribute to lists, requires prior specific permission.

**ARNOLD DIFFUSION IN WEAKLY COUPLED  
STANDARD MAPS**

by

B. P. Wood, A. J. Lichtenberg, and M. A. Lieberman

Memorandum No. UCB/ERL M90/42

24 May 1990

COVER PAGE

**ARNOLD DIFFUSION IN WEAKLY COUPLED  
STANDARD MAPS**

by

B. P. Wood, A. J. Lichtenberg, and M. A. Lieberman

Memorandum No. UCB/ERL M90/42

24 May 1990

**ELECTRONICS RESEARCH LABORATORY**

College of Engineering  
University of California, Berkeley  
94720

TITLE PAGE

**ARNOLD DIFFUSION IN WEAKLY COUPLED  
STANDARD MAPS**

by

**B. P. Wood, A. J. Lichtenberg, and M. A. Lieberman**

**Memorandum No. UCB/ERL M90/42**

**24 May 1990**

**ELECTRONICS RESEARCH LABORATORY**

**College of Engineering  
University of California, Berkeley  
94720**

# Arnold Diffusion in Weakly Coupled Standard Maps

B. P. Wood, A. J. Lichtenberg, and M. A. Lieberman

Department of Electrical Engineering and Computer Sciences

and the Electronics Research Laboratory

University of California, Berkeley, CA 94720

## ABSTRACT

The standard map has a divided phase space in which two dimensional regions of stochasticity are isolated by one dimensional KAM curves which form a barrier to diffusion in action. When two standard maps are coupled together, the two dimensional KAM surfaces no longer divide the four dimensional phase space, and particles diffuse slowly along stochastic layers by the process of Arnold diffusion. We compare an analytic calculation of the rate of localized Arnold diffusion with numerically determined rates in regions having rotational and librational KAM curves for a single map, in the weak coupling limit for which the three resonance model holds. We then determine the rate of global Arnold diffusion across many cells of the  $2\pi$  periodic mapping. The global diffusion rate depends both on the local diffusion rate and on the relative volume occupied by the various stochastically accessible regions in the four dimensional phase space.

# I. Introduction

In non-integrable Hamiltonian systems of more than two degrees of freedom, KAM curves cannot isolate the stochastic layers that lie along the separatrices of system resonances. That is, the entire web of stochastic layers are inter-connected, and initial conditions in any part of the web can ultimately diffuse to all parts of it. The process, first proved to exist by Arnold [1] and now known as Arnold diffusion, has been studied in a variety of problems.

If three resonances can be locally isolated to be of dominant importance, then a method exists for calculating the rate of diffusion along a local resonance layer, known as the three resonance or stochastic pump model. The model has been used to analytically predict the diffusion rate, with good agreement obtained with numerical results [2,3,4]. However, the thickness of the stochastic layer in action,  $\Delta I_s$ , produced by the interaction of the two strongest resonances, is exponentially thin in a perturbation parameter  $\epsilon$ :  $\Delta I_s \propto e^{-A/\epsilon^{1/2}}$ , ( $A \approx 1$ ). As  $\epsilon$  becomes small the interaction typically involves an increasing number of resonances, and the three resonance model under-estimates the diffusion.

An upper bound on the diffusion rate has been obtained by Nekhoroshev [5] of the form  $D = \langle \Delta I_s^2 \rangle / T \propto e^{-A/\epsilon^\gamma}$ , ( $A \approx 1$ ) where for the number of degrees-of-freedom  $N = 3$ ,  $\gamma = \frac{1}{8}$ , and therefore the diffusion may be quite rapid for relatively small  $\epsilon$ . In the regime where many resonances overlap, this scaling has been investigated numerically for a model problem, for  $N = 3$ , obtaining  $\gamma = \frac{2}{3}$  [6]. This scaling with  $\epsilon$  is intermediate between the three resonance model and the Nekhoroshev upper bound. All of the above results are

local, with the value of  $\epsilon$  associated with different resonant interactions varying widely over different regions of the phase space.

Alternatively, a different question can be asked in connection with Arnold diffusion, i.e., how long does it take for an initial condition to globally explore the phase space in a coarse-grained sense. Only the widest pathways of the Arnold web are considered to participate in the diffusive process in this macroscopic sense, and thus a three resonance model might be adequate, together with appropriate phase space averaging, to predict a global rate of diffusion. This procedure has been successfully used to compute the global diffusion rate through a stochastic web in a simpler problem [7].

In order to compare theory with numerical results, it is important (1) to investigate a problem for which the main resonances span the space in a coarse-grained sense, such that the dominant diffusion is along the main resonances, (2) that the diffusion is calculable, locally, from a three resonance model, and (3) that the structure of the phase space is globally regular. All of these conditions are satisfied by a pair of weakly coupled standard maps in which the action is not restricted to a torus. The standard map also is convenient in that it has been extensively studied and its structure is well known. Probably for this latter reason, there has been recent interest in the Arnold diffusion in such mappings [8,9,10].

The standard map, described by the equations

$$\begin{aligned} I_{n+1} &= I_n + K_i \sin \theta_n, \\ \theta_{n+1} &= \theta_n + I_{n+1}, \end{aligned} \tag{1}$$

has been very useful in studying Hamiltonian chaos. It has the important property of being  $2\pi$  periodic in both angle and action, this latter property being of particular importance for the study of diffusion [11,4]. In addition, many interesting maps can be locally approximated

by the standard map. As can be seen in Figure 1, generated by iterating a number of initial conditions with  $K_i = 0.8$ , the phase space consists of regions of stochasticity separated by regular motion on KAM curves. The KAM curves consist of two types, librational motion about fixed points and phase spanning rotational motion.

A four dimensional phase space can be produced by linking two standard maps together with a coupling term:

$$\begin{aligned}
 I_{n+1} &= I_n + K_i \sin \theta_n + \mu \sin (\theta_n + \phi_n), \\
 \theta_{n+1} &= \theta_n + I_{n+1}, \\
 J_{n+1} &= J_n + K_j \sin \phi_n + \mu \sin (\theta_n + \phi_n), \\
 \phi_{n+1} &= \phi_n + J_{n+1}.
 \end{aligned}
 \tag{2}$$

The one dimensional KAM curves in the single map (1) become two dimensional KAM tori in the coupled map (2). Since a two dimensional tori cannot divide a four dimensional phase space, there can be diffusion of particles around the KAM surfaces in the coupled map, which is the Arnold diffusion. The diffusion can be thought of as a random walk across KAM curves in one map due to the kicks in action delivered by a stochastic component of the phase motion of the other map. For small values of  $\mu$  this viewpoint allows a reasonably accurate calculation of the diffusion rate. as described in the next section. An example of the Arnold diffusion is shown in Figure 2. which is a projection onto the  $(I, \theta)$  and  $(J, \phi)$  phase spaces of the position of a phase point recorded over 9000 mapping periods. The initial condition in  $(J, \phi)$  explores the available stochastic phase space around the separatrix of the main island, but is transiently confined between KAM curves. The initial condition in  $(I, \theta)$  on a rotational KAM curve for the uncoupled map slowly diffuses to neighboring rotational

curves over a time long compared to the time for the  $(J, \phi)$  motion to define its stochastic separatrix region.

There will be three characteristic rates of diffusion in the coupled map. The first is the fast diffusion across stochastic layers, which occurs simultaneously in both actions when a particle is in the stochastic regions of both individual maps. The second is the Arnold diffusion driven by the main stochastic layer. Slower Arnold diffusion occurs when a particle is in a secondary stochastic layer in one map and on a KAM curve in the second map. For small values of the coupling parameter  $\mu$ , particles on regular orbits in both uncoupled maps are on a two dimensional KAM torus in the coupled system. In this case no diffusion occurs.

## II. Local Rate of Arnold Diffusion

We can calculate the rate of Arnold diffusion from the three resonance stochastic pump model [2,3,4] which we outline here. Assuming diffusion in the  $(I, \theta)$  map is driven by stochasticity in the  $(J, \phi)$  map, the Hamiltonian of the mapping is approximated as  $H \approx H_i + H_j$ , with

$$\begin{aligned} H_i &= \frac{I^2}{2} + K_i \cos \theta + 2\mu \cos(\theta + \phi), \\ H_j &= \frac{J^2}{2} + K_j \cos \phi + 2K_j \cos \phi \cos 2\pi n, \end{aligned} \tag{3}$$

where we have kept only the lowest fourier term from the mapping frequency in the  $H_j$  equation of (3), and considered that the stochasticity in  $H_i$  is driven by the coupling. To calculate the changes in  $H_i$  per iteration due to kicks delivered by  $(J, \phi)$ , we take the derivative

$$\frac{\partial H_i}{\partial n} = \frac{dH_i}{dn} = \frac{d}{dn} [2\mu \cos(\theta + \phi)] + 2\mu \frac{d\theta}{dn} \sin(\theta + \phi(n)). \tag{4}$$

The first term produces no net change over long times, and can be dropped. For rotational orbits we assume that  $\theta = \omega_i n + \theta_0$ , where  $\omega_i$  is a frequency which is approximately equal to the average action of the rotational KAM curve, and  $\theta_0$  is a phase. Scaling the “time” variable to revolutions of the map,  $s = \omega_j n$ , and defining the ratio of frequencies

$$Q_0 = \frac{\omega_i}{\omega_j} = \frac{\omega_i}{K_j^{1/2}}, \quad (5)$$

(4) is integrated to obtain

$$\begin{aligned} \Delta H_i &= \int_{-\infty}^{\infty} \frac{dH_i}{dn} \frac{dn}{ds} ds \\ &= 2\mu Q_0 \left[ \cos \theta_0 \int_{-\infty}^{\infty} \sin [Q_0 s + \phi(s)] ds + \sin \theta_0 \int_{-\infty}^{\infty} \cos [Q_0 s + \phi(s)] ds \right]. \end{aligned} \quad (6)$$

Since  $\phi(s)$  is an odd function, the first of the integrals in (6) integrates to zero. The second is a Melnikov-Arnold integral [2], which can be evaluated to produce the result

$$\Delta H_i = 8\pi\mu Q_0^2 \sin \theta_0 \frac{\sinh(\pi Q_0/2)}{\sinh(\pi Q_0)}.$$

Squaring  $\Delta H_i$  and averaging over  $\theta_0$  gives

$$\langle (\Delta H_i)^2 \rangle = 32\pi^2 Q_0^4 \mu^2 \frac{\sinh^2(\pi Q_0/2)}{\sinh^2(\pi Q_0)}. \quad (7)$$

This is the change in  $H_i$  over one characteristic half period of the  $(J, \phi)$  map. To determine the diffusion constant  $D$ , divide  $\langle (\Delta H_i)^2 \rangle$  by twice the average number of iterations in this half period,

$$\overline{T_j} = \frac{1}{\omega_j} \ln \left| \frac{32e}{w_1} \right|, \quad (8)$$

where  $w_1 = \frac{\Delta H}{H_{\text{separatrix}}}$  is the relative energy of the edge of the stochastic region,

$$w_1 = 8\pi \left[ \frac{2\pi}{K_j^{1/2}} \right]^3 e^{-\pi^2/K_j^{1/2}}. \quad (9)$$

Combining (7), (8), and (9), and using  $\Delta H_i = I \Delta I$ , the diffusion distance in action is

$$\begin{aligned} \Delta I_{rms} &= [ \langle (\Delta I)^2 \rangle n ]^{1/2} = \frac{[ \langle (\Delta H_i)^2 \rangle n ]^{1/2}}{2\overline{T}_j I} \\ &= \frac{4\pi\mu K_j^{1/4} n^{1/2} Q_0^2}{I \left[ \frac{3}{2} \ln K_j + \frac{\pi^2}{K_j^{1/2}} - 4.27 \right]^{1/2}} \frac{\sinh(\pi Q_0/2)}{\sinh(\pi Q_0)}. \end{aligned} \quad (10)$$

The range of values of  $I$  and  $K_j$  which are interesting numerically produce values of  $Q_0$  between 2 and 6. For these values of  $Q_0$ , (10) can be approximated in a form which exhibits the main  $Q_0$  scaling:

$$\Delta I_{rms} \approx 4\mu n^{1/2} Q_0 e^{-\pi Q_0/2}, \quad (11)$$

where we have assumed in (10) that  $I \approx \omega_j$  and that  $\pi^2/K_j^{1/2}$  is the dominant term of the square root in the denominator.

These analytic results can be compared with the numerically determined diffusion distances. Some typical numerical results plotting  $\Delta I_{rms}$  versus  $n$  for a few representative values of  $\mu$  and  $Q_0$  are shown in Figure 3. The initial conditions for 200 particles were taken on the KAM curve with a rotation number of the golden mean in the  $(I, \theta)$  space, and in the primary stochastic region in the  $(J, \phi)$  space. The slopes on the log-log scale are  $\frac{1}{2}$ , and the heights are proportional to  $\mu$ , both characteristic of the scaling in (11). For these cases we might expect the local diffusion formula to hold. The numerical calculations are terminated at  $\Delta I_{rms} = 0.2$  to keep the diffusion local.

In Figure 4 the analytic value for  $\Delta I_{rms}$  from (10) is compared with the numerically computed values after  $2^{18}$  iterations for a single  $\mu$  and a variety of values for  $K_i$  and  $K_j$ . The analytic curve for a fixed  $\mu$  and  $n$  depends only on  $Q_0$  and therefore corresponds to all values of  $K_j$ . The exponential dependence on  $Q_0$  in (11) is clearly observed. In all these curves,

the particles in  $(I, \theta)$  were started on the KAM curve with a rotation number equal to the golden mean (0.618...). This KAM curve was chosen because it is far from sizable island chains which would distort the diffusion calculation. Numerically there is a weak dependence on  $K_i$ , with the large  $K_i$  curves lying above the small  $K_i$  curves. A possible explanation is that the rotational KAM curves have larger variations in action for larger values of  $K_i$ . Our analytic value for  $\Delta I_{rms}$  was derived using an average value of  $\omega_i$  for these curves. However, since  $\omega_i$  enters into (10) exponentially through  $Q_0$ , the use of an average frequency would tend to underestimate  $\Delta I_{rms}$ .

The calculation of the diffusion across the librational curves is done similarly to (3) through (10), except that for a librational curve  $\theta = \theta_0 \cos(\omega_i n + \chi_0)$ , where  $\omega_i = K_i^{1/2}$ ,  $\chi_0$  is a phase, and  $\theta_0$  is the maximum angle of the librational orbit. The calculation involves an expansion for small  $\theta_0$  and is therefore more involved. A quite similar calculation can be found in reference [4]. The result is

$$\Delta I_{rms} = \frac{4\pi\mu K_j^{1/4} n^{1/2} \theta_0 Q_0^2}{I \left[ \frac{3}{2} \ln K_j + \frac{\pi^2}{K_j^{1/2}} - 4.27 \right]^{1/2}} \frac{\sinh(\pi Q_0/2)}{\sinh(\pi Q_0)} \quad (12)$$

which looks like (10), except that it includes  $\theta_0$ , and  $Q_0 = \left(\frac{K_i}{K_j}\right)^{1/2}$  depends on  $K_i$ . As in the rotational case, we can approximate (12) to emphasize the main  $Q_0$  dependence. The approximate result does not depend on  $\theta_0$ , because  $\theta_0 K_i^{1/2}/I \approx 1$  over a wide range of  $\theta_0$  and  $K_i$ . The result is the same as in the rotational case:

$$\Delta I_{rms} \approx 4\mu n^{1/2} Q_0 e^{-\pi Q_0/2}.$$

However, the range of  $Q_0$  is now from 0.5 to 1.5, which produces quite different rates of diffusion than in the rotational case.

In Figure 5 we present a numerical calculation of  $\Delta I_{rms}$  versus  $n$  for libration orbits, using the same parameters as in Figure 3, except that  $\theta_0 = 0.2$ ,  $I_0 = 0$  for the initial conditions in the  $(I, \theta)$  plane. We now note some significant anomalies from the expected behavior. For the larger values of  $\mu$  the diffusion rate does not scale proportional to  $\mu$ . For the smaller  $K_j$ , there is a more dramatic effect at large  $\mu$ , with non-diffusive behavior observed. We believe these effects are due, in part, to a reordering of the resonance strengths that occurs for large coupling, and possibly also related to a change in phase space structure that appears near the origin of the main resonance [9]. We stay away from these anomalies in comparing the theory and numerics for local diffusion on librational orbits, by choosing  $\mu$  sufficiently small.

In Figure 6 the analytic value for  $\Delta I_{rms}$  from (12) is compared with the numerically computed values after  $2^{18}$  iterations for a variety of values for  $K_i$  and  $K_j$ . In these curves, the particles in  $(I, \theta)$  were started on the librational KAM curve with  $\theta_0 = 0.2$ ,  $I_0 = 0$ . Note that (12) is parameterized by  $K_j$  rather than by  $K_i$  as was the case in (10). The analytical curve appears to form an upper bound on the numerical curves and appears to agree most closely at the larger values of  $K_j$ . For smaller values of  $K_j$ , the numerically computed curve lies below the analytical curve. Further numerical work has shown that this reduction for small  $K_j$  is even greater for larger values of  $\theta_0$ . However, for the global diffusion calculation in the next section, the librational orbits play a role in the calculation that does not depend on their local diffusion rate, so this disagreement between numerical calculation and theory will not concern us for that calculation.

### III. Global Rate of Arnold Diffusion

We now examine the global diffusion in action across the entire phase space for a large number of iterations. An example of this diffusion in action is shown for  $K_i = K_j = 0.8$  and  $\mu = 0.01$  on a surface of section at  $\theta = \phi = \pi$  in Figure 7. This is not simply a trivial extension of our local results to large  $n$ , because the diffusion carries the particles across island chains and into regions of different  $I$ .

We will formulate an intuitive model of how the global diffusion proceeds. Assume a particle starts in the primary stochastic regions of both the  $(I, \theta)$  and  $(J, \phi)$  maps. The particle will explore this double stochastic region until it is kicked out onto a nearby KAM curve in one of the maps, say, a rotational curve in  $(I, \theta)$ . The stochasticity in  $(J, \phi)$  will then drive Arnold diffusion across the rotational curves in  $(I, \theta)$ . This corresponds to motion along one of the major horizontal lines away from one of the four central “blobs” in Figure 7. Eventually, the particle will encounter another stochastic region in  $(I, \theta)$ . For instance, in the  $K = 0.8$  case shown in Figure 7, the next stochastic region of substantial size will be that surrounding the island chain with four islands and a rotation number of  $1/4$  (see Figure 1). The particle will then explore this double stochastic region until it is again kicked out onto a nearby KAM curve. In the case at hand, it is most likely that the primary stochastic region in  $(J, \phi)$  would kick the particle off the “ $1/4$ ” stochastic region in  $(I, \theta)$ , but there is a possibility (in the ratio of the kick sizes) that the opposite will happen. In the latter case, the “ $1/4$ ” stochastic region in  $(I, \theta)$  will begin driving Arnold diffusion across KAM curves in  $(J, \phi)$ . It is by this process that the interior of some of the “squares” in Figure 7 are filled

in. The particle will continue this process of hopping from one stochastic layer to another as it diffuses along the various layers in the  $(I, J)$  plane.

The kick size delivered by a stochastic region is proportional to the width of the stochastic region. Since the phase space of the angle variable is limited to  $2\pi$ , the kick size is also proportional to the area of the stochastic region. These quantities are exponentially small in the ratio of the local frequency to the mapping frequency for the uncoupled map. In the coupled map, there are coupling resonances which thicken the stochastic regions. This thickening is demonstrated in Figure 8, which shows the total area covered by the stochastic region, for island chains of differing periodicities, without coupling and with a coupling of  $\mu = 0.003$  and  $\mu = 0.01$ . In Figure 8 we have taken into account the differing multiplicities of island chains of differing periodicity, ie., that there are two island chains which have four islands (rotation numbers  $1/4$  and  $3/4$ ) versus four island chains which have seven islands (rotation numbers  $2/7$ ,  $3/7$ ,  $4/7$ , and  $5/7$ ). Note that the relative thickening is greater for thin (larger period) island chains. This suggests that the thin stochastic regions can deliver a larger kick than would be expected from their thickness in the uncoupled map, increasing the likelihood that they drive Arnold diffusion by kicking a particle out of a larger stochastic region in the other map of the coupled system. They can also store a significant number of particles in stochastic layers in which the diffusion is relatively slow, which will be the important property for our global diffusion calculation. Although the total area of the  $\mu$  thickened stochastic regions does not appear to be converging to a particular value in Figure 8 we find that island chains with periodicity higher than eight tend to have been absorbed by  $\mu$  thickened stochastic regions of lower periodicity. By carrying our summation of stochastic

region area out to periodicity nine island chains, we feel we have accounted for almost all of the stochastic area.

We can check this result by counting the number of particles in the various portions of the stochastic web. Figure 9 shows the  $(I, J)$  plane at a surface of section through  $\theta = \phi = \pi$  for 1000 particles iterated 2 million times each. In this figure  $K_i = K_j = 0.8$  and  $\mu = 0.003$ . The  $(I, J)$  plane has been made  $2\pi$  periodic to show the detail of the diffusion. The particles are superimposed upon a grid which shows the stochastic regions at this surface of section around the island chains which have 1, 2, 3, and 4 islands. The width of the stochastic region is resolved only for the primary island. The clustering of the particles positions near the stochastic layers indicates the particles are diffusing along this grid. Using Figure 9 and similar results for  $\mu = 0.01$ , shown in Figure 10, we can test a key requirement of our global diffusion calculation: that the phases space is reasonably filled on the time scales of the numerical calculation. For  $\mu = 0.01$ , in Figure 10, 33% of the particles are in the primary stochastic region of either map, and the phase space appears to be uniformly populated. Referring to Figure 8, we find that for  $\mu = 0.01$ , about 39% of the stochastic phase space is in the primary stochastic region. Although this figure is slightly high, we expect the inclusion of the stochasticity of the remaining higher periodicity island chains would make it fully consistent with the value from Figure 10. In contrast, for  $\mu = 0.003$ , in Figure 9, 55% of the particles are in the primary stochastic region of either map, and the phase space is not uniformly populated. Referring to Figure 8, we find that for  $\mu = 0.003$ , about 52% of the stochastic phase space is in the primary stochastic region. As in the previous case, we expect the actual figure to be somewhat lower. The fact that more particles remain in the

primary stochastic regions in Figure 9 than is predicted by Figure 8 is consistent with the phase space not being uniformly populated for  $\mu = 0.003$  after two million iterations.

As noted above, the stochastic regions are exponentially thin in  $K$ . However, there is an additional variation with  $K$  and position in the phase plane which should be noted. As  $K$  is increased, big stochastic regions absorb smaller stochastic regions. For instance, at  $K \approx 0.76$  the stochastic region around the island chain with rotation number  $1/5$  merges with and becomes part of the primary stochastic region. Before undergoing this merge, the  $1/5$  stochastic region itself thickens by absorbing still smaller stochastic regions which lie between it and the primary stochastic region. This process continues to smaller scales, with a renormalization scaling [12]. In this way, the stochastic regions are extended across the map until, at  $K \approx 0.9716$ , the last rotational KAM curve disappears (specifically, the one with the golden mean rotation number) and a stochastic path extends across the entire map in action. The importance of this to our investigation is that the phase space accessible from a particular stochastic location increases with  $K$  irregularly, and hence the rate of Arnold diffusion may change substantially with a small change in  $K$ . It should also be noted that the multiple examples of a particular period island chain will not necessarily have the same size stochastic region. For instance, we might expect the stochastic regions of the island chains with rotation numbers  $2/7$  and  $3/7$  to be of the same size. We have numerically determined that the  $2/7$  stochastic region has an area that is 4.8 times that of the  $3/7$  island chain at  $K = 0.8$  in the uncoupled map. Similarly, the  $2/9$  island chain has an area equal to 29 times that of the  $4/9$  island chain. These irregularities should be more evident in the local diffusion calculations than in the global diffusion calculations, where they will tend to be smoothed.

When a particle diffuses into a resonance zone consisting of libration orbits surrounded by a stochastic layer, it is quickly transported across the island chain. There is also some probability of diffusing more deeply into the central librational area. Diffusion across librational curves differs from that across rotational curves in two important ways beside the difference in  $Q_0$ . First, the second order island chains within a librational region are much smaller than the higher period island chains in the rotational regions. Second, because the librational orbits encircle a singular elliptic fixed point, there is less phase space in the inward direction than in the outward direction. Thus there will be fewer particles at smaller values of action in the librational region of the primary resonance. This fall off in density can be seen in Figure 10 as a relative absence of particles in the regions where  $I$  or  $J$  are near 0 or  $2\pi$ . The near total absence of particles in the four corners (a typical region is labeled with an "A") corresponds to particles being on librational orbits within the primary stochastic region in both of the maps. Similarly, there are empty regions in Figure 10 at all combinations librational-librational regions inside the island chains as well (typical regions are labeled with a "B").

The net effect of the librational phase space within the stochastic layer in calculating the overall global diffusion is that it stores particles that do not actively diffuse. In other words, the librational phase space removes a portion of the particles from the global diffusion, but the remaining particles can be considered to jump over this phase space in diffusing across the  $(I, J)$  phase plane by passing through the stochastic regions around the librational regions. This librational phase space can account for a substantial portion of the total phase space. In the uncoupled map, we have determined numerically that the fraction of the phase space

which is librational scales approximately linearly with  $K$  between  $K = 0.2$  and  $K = 0.7$  and reaches a maximum of about 50% at  $K = 0.8$ , as shown in Figure 11.

A summary of the four types of coupled phase space is given below:

1. **Stochastic-stochastic:** a particle in this region is immediately transported a distance in action equal to the width of the island chain around which the stochastic region lies. Particles in this region contribute to the diffusion, but with a very high diffusion rate.
2. **Stochastic-librational:** the motion of a particle in this region averages to the fixed point as it librates around the island. It is therefore effectively removed from the global diffusion while in this region.
3. **Stochastic-rotational:** a particle Arnold diffuses slowly through this region until it encounters another stochastic region in the rotational map. We divide this region into two classes: (a) the primary stochastic layer and (b) regions other than the primary layer for which the diffusion is very slow, and to first order can be ignored.
4. **Regular-regular:** particles which begin in a stochastic region in at least one of the maps cannot diffuse into these regions. This phase space is removed from the calculation of global diffusion.

The following method is suggested to calculate the global diffusion. A diffusion rate along the stochastic layers of the primary island chain is calculated by averaging the local Arnold diffusion rate across regions 1 and 3(a). Regions 2 and 3(b) act as sinks for particles, removing them from the diffusion process. Region 4 is omitted from the calculation.

The local diffusion constant,  $D_l$ , varies greatly with  $\omega_i \approx I$ , as shown in Figure 12. To determine an average diffusion constant,  $D_{ave}$ , over a  $2\pi$  interval, we must average the reciprocal of  $D_l$  across the regions participating in the diffusion. The diffusion through the

stochastic regions is very fast, so it will contribute little except it's area to  $D_{ave}$ . Due to the symmetry of the map about  $I = \pi$ , we need only calculate the average for half the map, so we take as the limits of our integration the edges of the primary and period 2 island chain stochastic regions, as shown in Figure 1. The integration is:

$$\left\langle \frac{1}{D_{ave}} \right\rangle = \frac{1}{\pi} \frac{\frac{3}{2} \ln K_j + \frac{\pi^2}{K_j^{1/2}} - 4.27}{K_j^{1/2} (4\pi\mu/K_j)^2} \int_{.42\pi}^{.92\pi} \frac{\sinh^2(\pi\omega_i/K_j^{1/2})}{\sinh^2(\pi\omega_i/2K_j^{1/2})} \omega_i^{-4} d\omega_i.$$

This equation can be evaluated numerically to produce  $D_{ave} = \langle 1/D_{ave} \rangle^{-1} = 5.8 \times 10^{-5}$  for  $K_j = 0.8$  and  $\mu = 0.01$ . To produce the proper global diffusion constant we must weight the average diffusion constant by the proportion of particles that actually participate in the diffusion:

$$D_g = \frac{N_{dif}}{N_{tot}} D_{ave}. \quad (13)$$

To determine  $N_{dif}$ , we need to numerically calculate the relative areas of the librational, rotational, and stochastic regions of a single map with coupling-resonance-thickened stochastic regions. For  $K_j = K_i = 0.8$  and  $\mu = 0.01$ , we find that approximately 40% is librational, 11% is rotational, 19% is primary stochastic, and 30% is secondary stochastic. In making this numerical calculation, we have included island chains with period  $\leq 9$ . Since we have two maps, we multiply out the various combinations of these regions and sum over like regions, finding that 26% of the phase space is in regular (ie., librational or rotational) regions in both maps. No particles diffuse into the regular-regular regions, so we remove that phase space from the calculation. Of the remaining phase space, 32% is stochastic-stochastic, 6% is primary stochastic-rotational, 9% is secondary stochastic-rotational, and 53% is stochastic-librational. The 32% stochastic-stochastic phase space can be subdivided

into primary-primary (5%), primary-secondary (15%), and secondary-secondary (12%) regions.

Only those particles in the primary-primary, primary-secondary, and primary stochastic-rotational regions will contribute to the diffusion. Assuming that all regions are uniformly populated with particles in the limit of long times, we find that  $\frac{N_{diff}}{N_{tot}} \approx 0.26$ . Substituting this value into (13) gives  $D_g \approx 1.5 \times 10^{-5}$ . Similarly, for  $\mu = 0.003$  we obtain  $\frac{N_{diff}}{N_{tot}} \approx 0.29$  and  $D_g \approx 1.5 \times 10^{-6}$ .

The expected diffusion distance is then

$$\Delta I_{rms} = \frac{(nD_g)^{1/2}}{\langle I \rangle}, \quad (14)$$

where  $\langle I \rangle \approx \frac{\pi}{2}$ . The resulting  $\Delta I_{rms}$  is compared to the numerically determined value as a function of the number of iterations  $n$  for 1000 particles with  $K_i = K_j = 0.8$  and  $\mu = 0.01$  and  $0.003$  in Figure 13.

The initial flat portion of the numerical curve is the result of all particles immediately taking on an action value equal to the width of the primary stochastic region at our surface of section  $\theta = \phi = \pi$ . As the particles diffuse outward and distribute themselves more evenly over the accessible phase space the numerical curve approaches the theoretical curve predicted by (14). The numerical curve remains some distance above the theoretical curve, because the theoretical curve was derived assuming that particles evenly fill the accessible phase space. In reality, there is a transient region at the outer edge of the diffusion where this even distribution has not been established. However, for long enough times the effect of this transient region will become negligible. We can estimate the time required for this to happen by examining the relative rates of Arnold diffusion driven by primary and secondary

stochastic regions. Define two characteristic diffusion times as  $t = L^2/D_f$  and  $\Delta t = \ell^2/D_s$ , where  $L$  is the long diffusion distance over the  $(I, J)$  phase plane,  $D_f$  is the fast rate for Arnold diffusion driven by the primary stochastic region along the stochastic grid shown in Figure 7,  $\ell \approx \pi/2$  is a characteristic short diffusion distance to fill in square regions “inside” the stochastic grid in Figure 7, and  $D_s$  is the slow rate for Arnold diffusion driven by the secondary stochastic regions.  $\Delta t$  is the characteristic time required to fill in the square regions “inside” the stochastic grid. We then have  $L'^2 = D_f(t + \Delta t)$ , where  $L'$  is the distance fast particles diffuse after an additional time  $\Delta t$ . Letting  $\Delta L = L' - L$ , we see that

$$L'^2 - L^2 \approx 2L\Delta L = D_f \frac{\ell^2}{D_s}.$$

Dividing through by  $L^2$ , we find

$$\frac{\Delta L}{L} \approx \frac{1}{2} \frac{\Delta t}{t},$$

so that the diffusion distance due to the transient effect,  $\Delta L$ , will be negligible after a time which makes  $\Delta t/t$  small. The time required to make  $\Delta L$  negligible will be greater for small  $\mu$ , because, as shown in Figure 8, the width of the primary stochastic region that drives the fast Arnold diffusion along the stochastic grid depends weakly on  $\mu$ , whereas the widths of the secondary stochastic regions depend strongly on  $\mu$ . It is these secondary stochastic regions that drive the slow Arnold diffusion which fills the squares inside the stochastic grid.

## IV. Conclusions

We have calculated local rates of Arnold diffusion across rotational and librational KAM curves in a system of coupled standard maps, for small coupling, employing a three resonance, stochastic pump model. Using these rates together with general arguments concerning

different classes of diffusing particles and the assumption that the long-time limit gives a uniform density in the accessible phase space, we have calculated a global rate of Arnold diffusion across the phase space on the action scale of  $2\pi$  at which the mapping equations are periodic. The numerically determined rates of both the local and global diffusion are in reasonable agreement with analytical calculations. Some anomalies exist, particularly in the local rate of diffusion across librational orbits, which merit further investigation. Two extensions of this work are to make similar calculations for large coupling, and to increase the number of degrees of freedom by coupling together a larger number of standard maps [13].

We gratefully acknowledge the support of ONR Grant N00014-84-K-0367 and NSF Grant ECS-8517364 for this work.

## References

- [1] V. I. Arnold, *Russian Mathematics Surveys* 18 85 (1964).
- [2] B. V. Chirikov, *Physics Reports* 52 263 (1979).
- [3] J. L. Tennyson, M. A. Lieberman, and A. J. Lichtenberg,  
*Nonlinear Dynamics and the Beam-Beam Interaction*, AIP Conference Proceedings No. 57  
272, American Institute of Physics N. Y. 1979.
- [4] A. J. Lichtenberg and M. A. Lieberman, *Regular and Stochastic Motion* Springer-Verlag  
N. Y. 1983.
- [5] N. N. Nekhoroshev, *Russian Mathematics Surveys* 32 6 (1977).
- [6] B. V. Chirikov, J. Ford, and F. Vivaldi, *Nonlinear Dynamics and the Beam-Beam Interaction*,  
AIP Conference Proceedings No. 57 323, American Institute of Physics N. Y. 1979.
- [7] Allan J. Lichtenberg and Blake P. Wood, *Physical Review A* 39 2153 (1989).
- [8] Kunihiko Kaneko and Richard J. Bagley, *Physics Letters* 110A 435 (1985).
- [9] G. Györgyi, F. H. Ling, and G. Schmidt, *Physical Review A* 40 5311 (1989).
- [10] G. R. Wang and B. Hu, private communication.
- [11] A. B. Rechester, M. N. Rosenbluth, and R. B. White, *Physical Review A* 23 2664  
(1981).
- [12] A. J. Lichtenberg, *Physica* 14D 387 (1985).
- [13] K. Kaneko and T. Konishi, *Physical Review A* 40 6130 (1989); see also T. Konishi and  
K. Kaneko, "Diffusion in Hamiltonian Chaos and its Size Dependence" Dept. Phys.  
Nagoya Univ. Report DPNU-90-19 (1990).

## Figure Captions

Figure 1. The standard map for  $K = 0.8$  and a number of initial particle positions. The bracket shows the region between the primary and period 2 island chains in which rotational KAM curves exist.

Figure 2. The coupled standard map for 9000 iterations of a single particle, projected onto the  $(I, \theta)$  and  $(J, \phi)$  planes. The particle was started in the primary stochastic region in  $(J, \phi)$ , and on the golden mean rotational KAM curve in  $(I, \theta)$ .

Figure 3. Arnold diffusion distance,  $\Delta I_{rms}$ , versus number of iterations for 200 particles and differing values of  $\mu$  and  $K_j$ , when particles are started on a rotational KAM curve in  $(I, \theta)$ .

Figure 4. Arnold diffusion distance,  $\Delta I_{rms}$ , after  $2^{18}$  iterations versus  $Q_0$ , for 200 particles,  $\mu = 0.0001$ , and differing values of  $K_i$ , when particles are started on a rotational KAM curve in  $(I, \theta)$ .

Figure 5. Arnold diffusion distance,  $\Delta I_{rms}$ , versus number of iterations for 200 particles,  $\theta_0 = 0.2$ , and differing values of  $\mu$  and  $K_j$ , when particles are started on a librational KAM curve in  $(I, \theta)$ .

Figure 6. Arnold diffusion distance,  $\Delta I_{rms}$ , after  $2^{18}$  iterations versus  $Q_0$ , for 200 particles,  $\theta_0 = 0.2$ ,  $\mu = 0.0001$ , and differing values of  $K_j$ , when particles are started on a librational KAM curve in  $(I, \theta)$ .

Figure 7. Arnold diffusion in the  $(I, J)$  phase plane for a surface-of-section at  $\theta = \phi = \pi$ , with  $K_i = K_j = 0.8$  and  $\mu = 0.01$ . 500 particles were started in the primary stochastic regions of both  $(I, \theta)$  and  $(J, \phi)$ , and run for two million iterations.

Figure 8. Area of the stochastic regions around island chains of varying periodicities for  $K_i = K_j = 0.8$ . Values are plotted for the uncoupled map, and for the coupled map with  $\mu = 0.01$  and  $0.003$ . Each value is the total area for all island chains of a particular periodicity, ie., there is a single island chain each with periods 1 and 2, there are two island chains each with periods 3, 4, 5, and 8, there are four island chains each with periods 7 and 9, and there are no island chains with period 6. The “missing” island chains of each periodicity either lie on top of a lower period island chain, or have been absorbed into the stochastic region around a lower period island chain. Areas are normalized to 1.

Figure 9. Arnold diffusion in the  $2\pi$  periodic  $(I, J)$  phase plane for a surface-of-section at  $\theta = \phi = \pi$ , with  $K_i = K_j = 0.8$  and  $\mu = 0.003$ . 1000 particles were started in the primary stochastic regions of both  $(I, \theta)$  and  $(J, \phi)$ , and run for two million iterations. The particles are superimposed upon a grid showing the primary stochastic region and the stochastic regions around the period 2, 3, and 4 island chains in the uncoupled map.

Figure 10. Same as Figure 9, except  $\mu = 0.01$ . The region labeled “A” is in the primary librational region in each map. The regions labeled “B” are in the period 2 island chain librational region in one or both maps.

Figure 11. The total librational area inside all island chains of the uncoupled map as a function of  $K$ . Areas are normalized to 1.

Figure 12. The local Arnold diffusion constant,  $D_l$ , for rotational orbits as a function of  $\omega_i \approx I$  for  $K_i = 0.8$ . It is normalized so the maximum  $D_l = 1$ .

Figure 13. The numerically calculated global Arnold diffusion distance is compared with the theoretical value, versus number of iterations, for  $K_i = K_j = 0.8$  and  $\mu = 0.01$  and  $0.003$ . 1000 particles were started in the primary stochastic regions of both  $(I, \theta)$  and  $(J, \phi)$ .

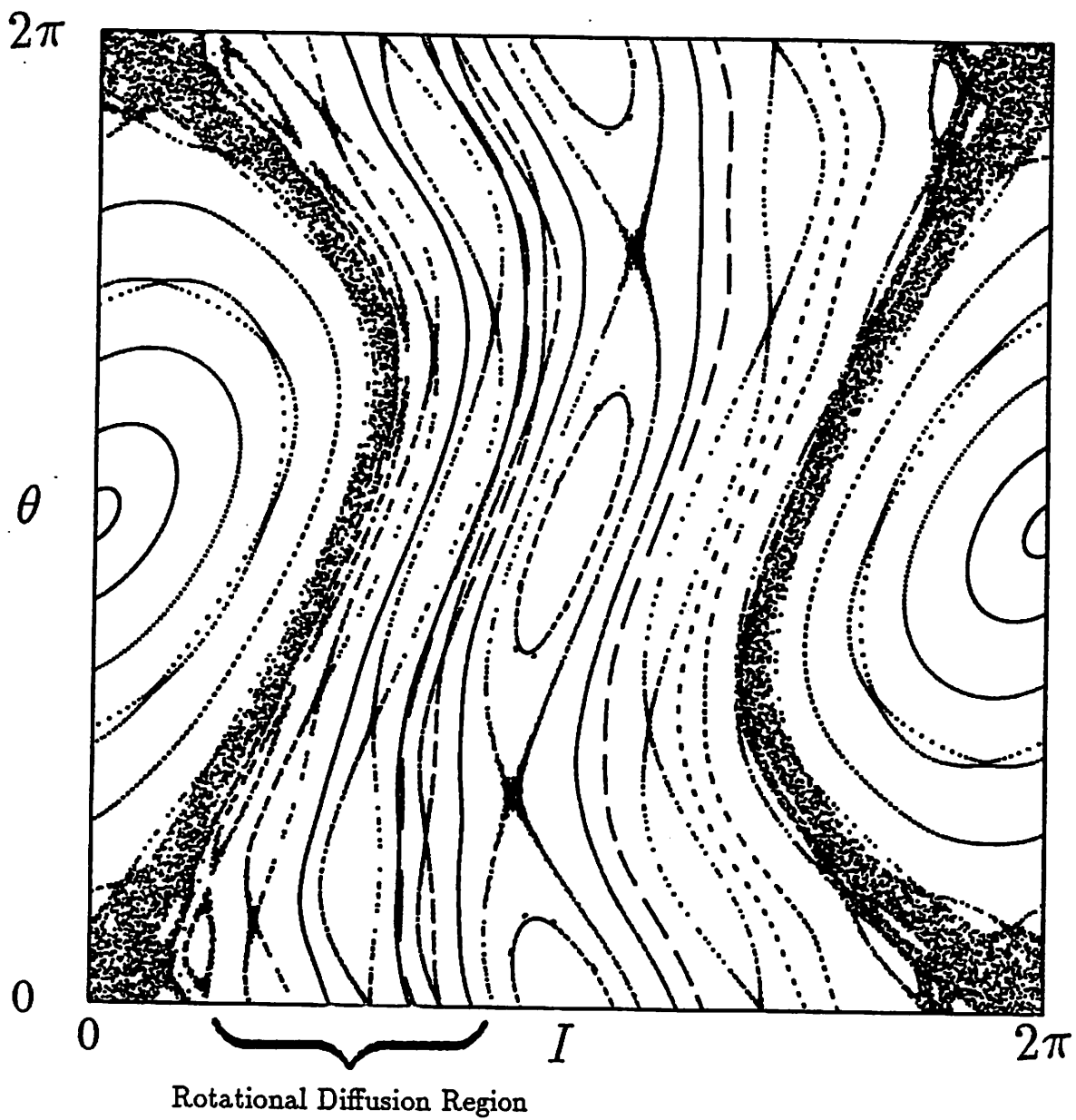
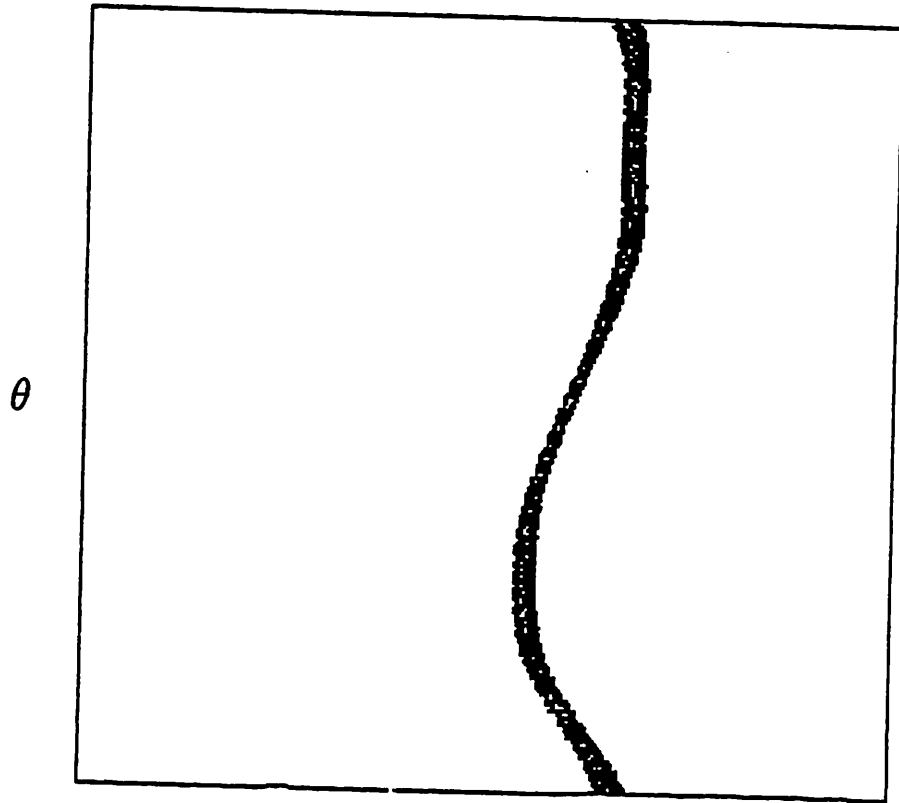
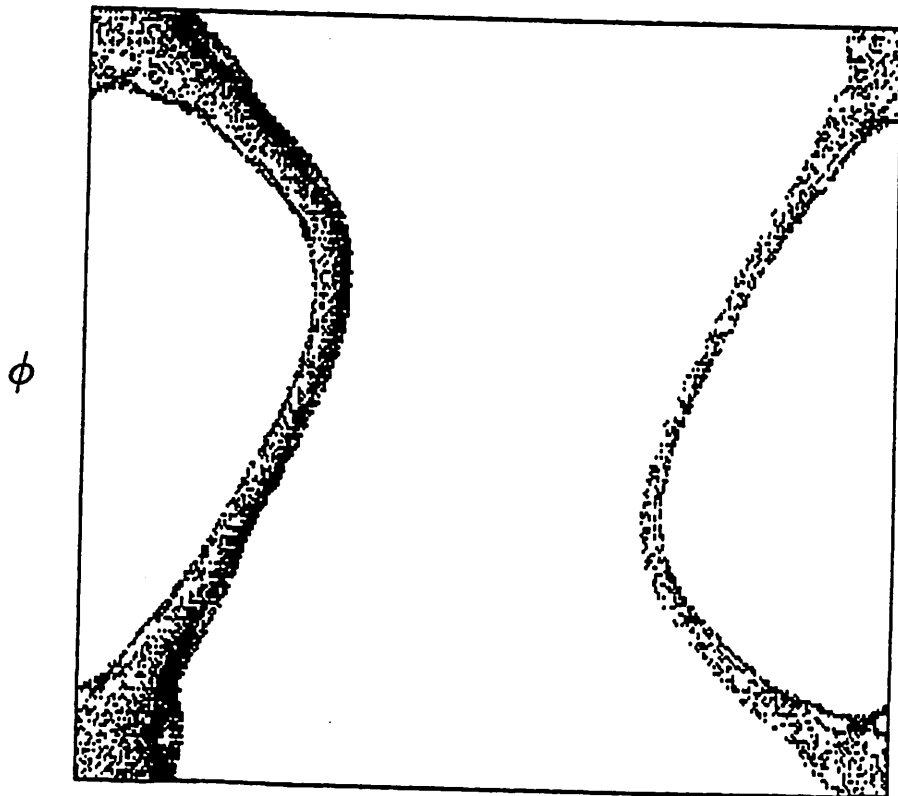


Figure 1



*I*



*J*

Figure 2

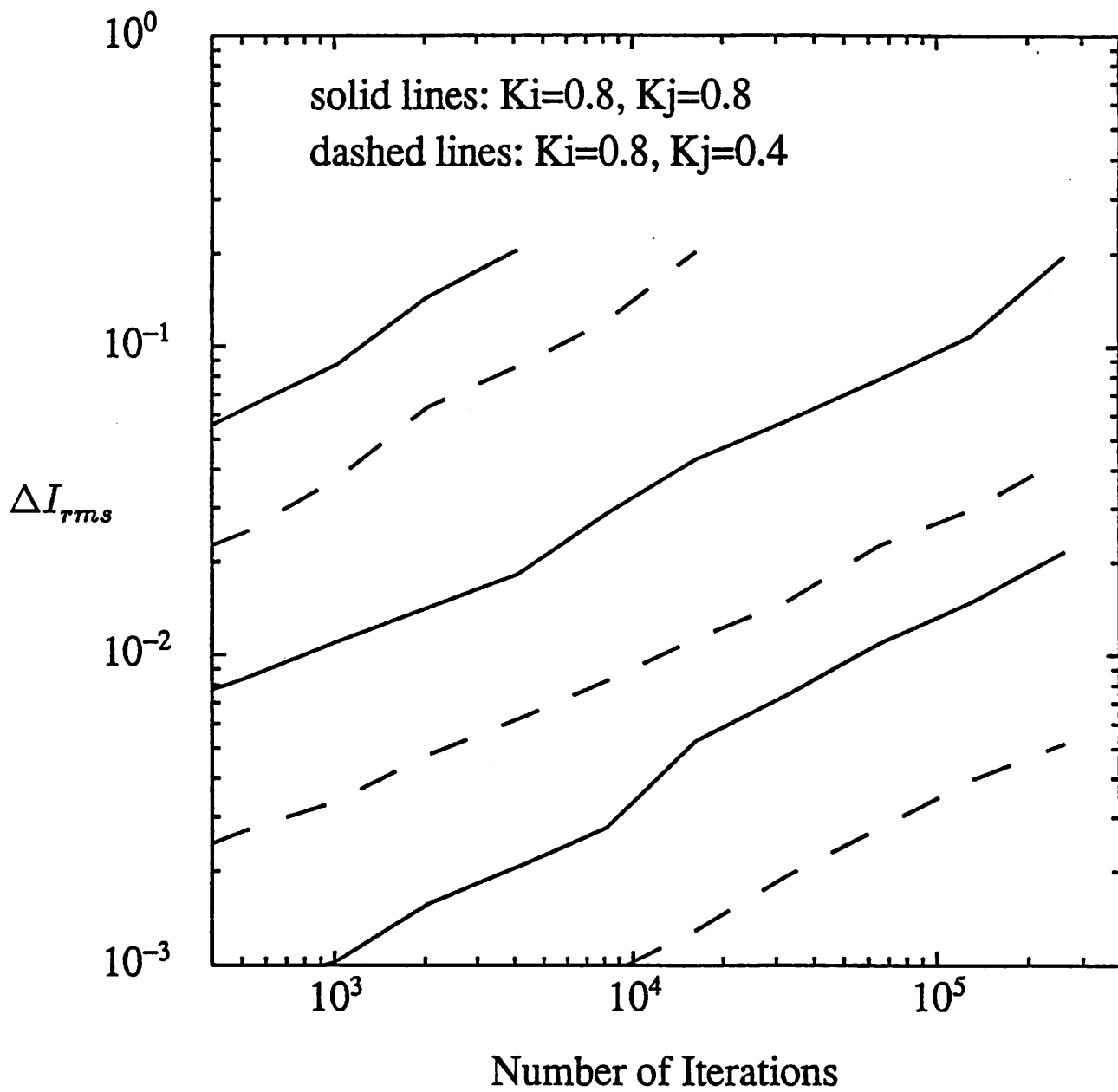


Figure 3

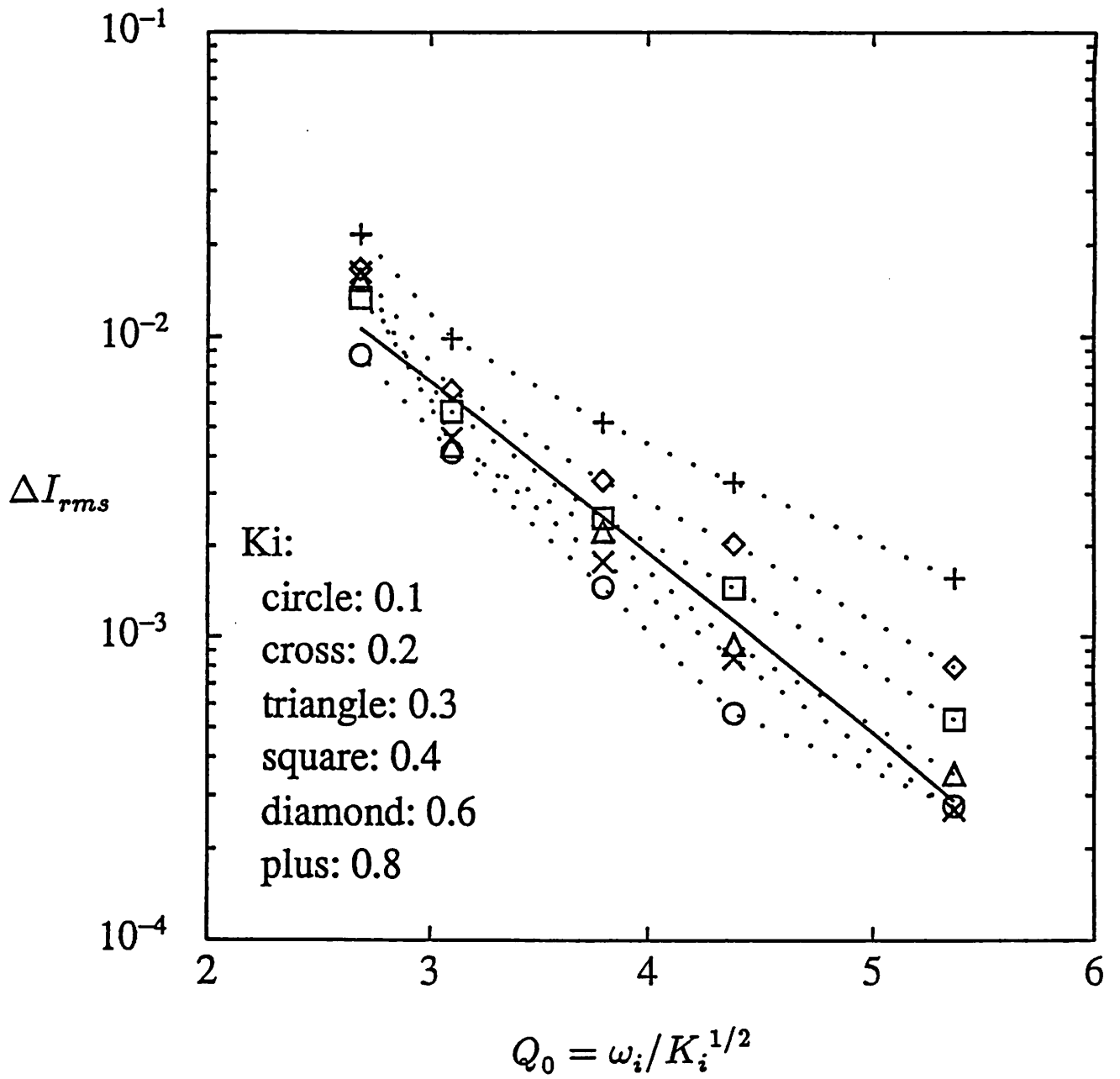


Figure 4

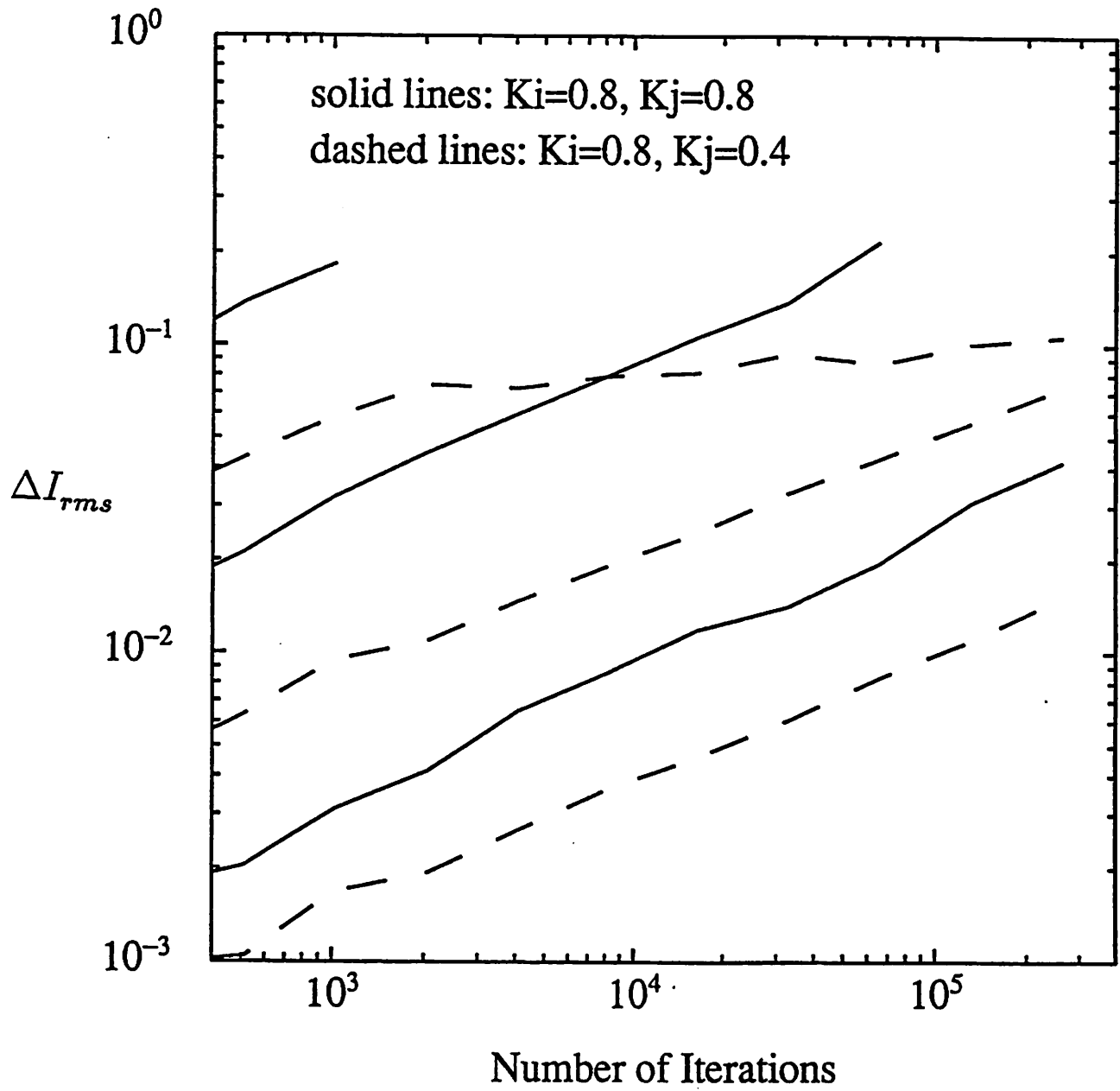


Figure 5

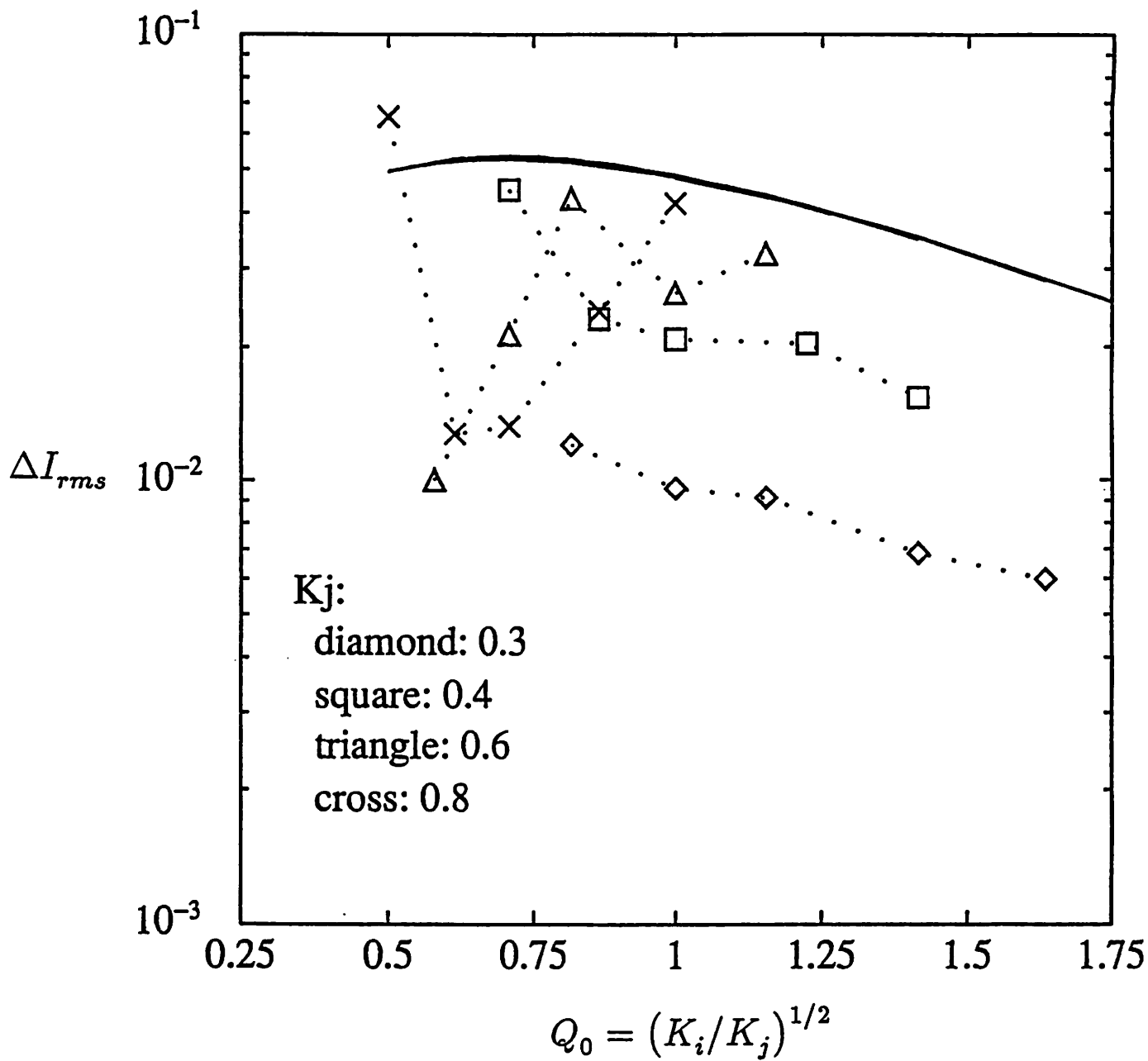


Figure 6

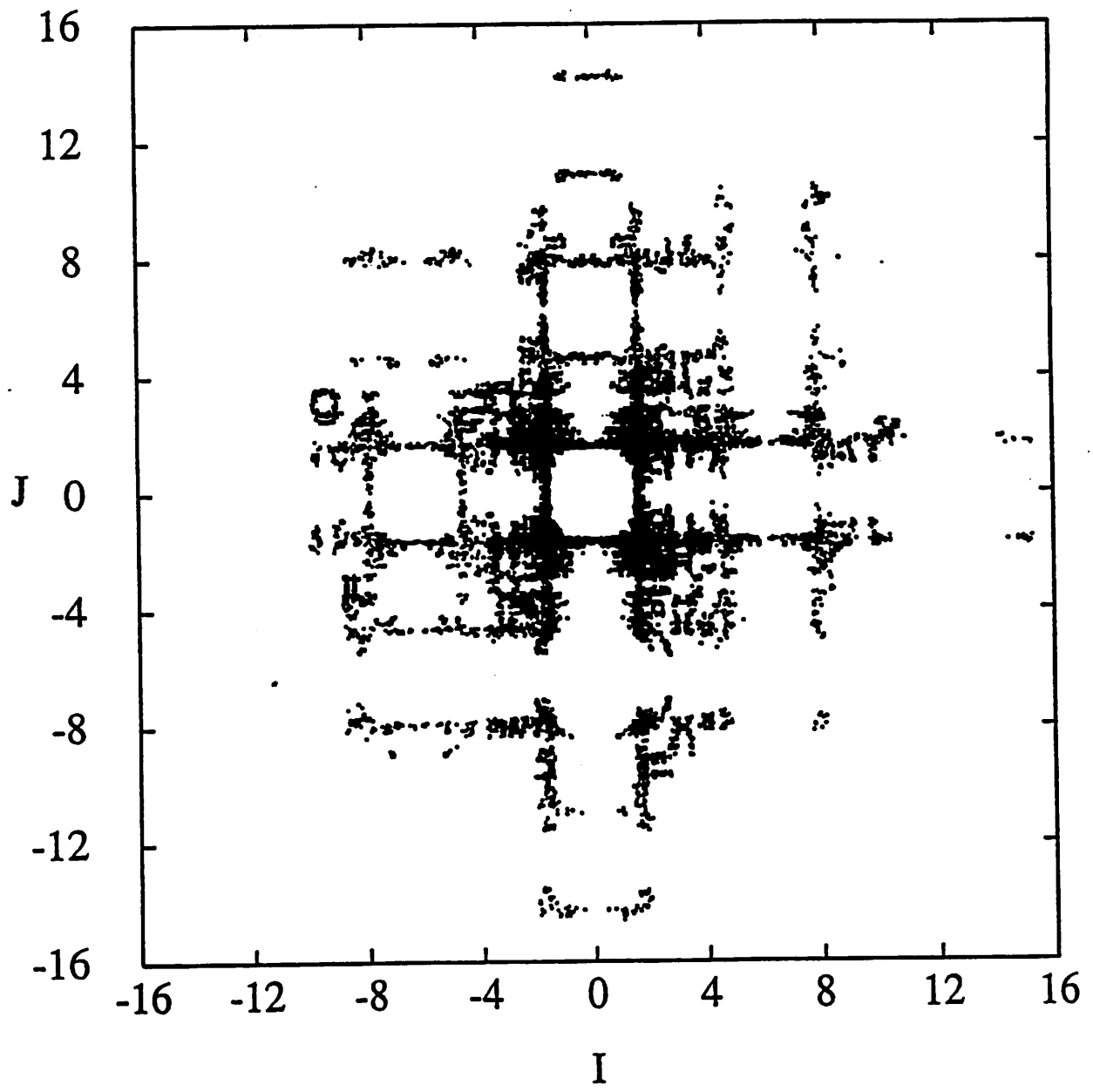


Figure 7

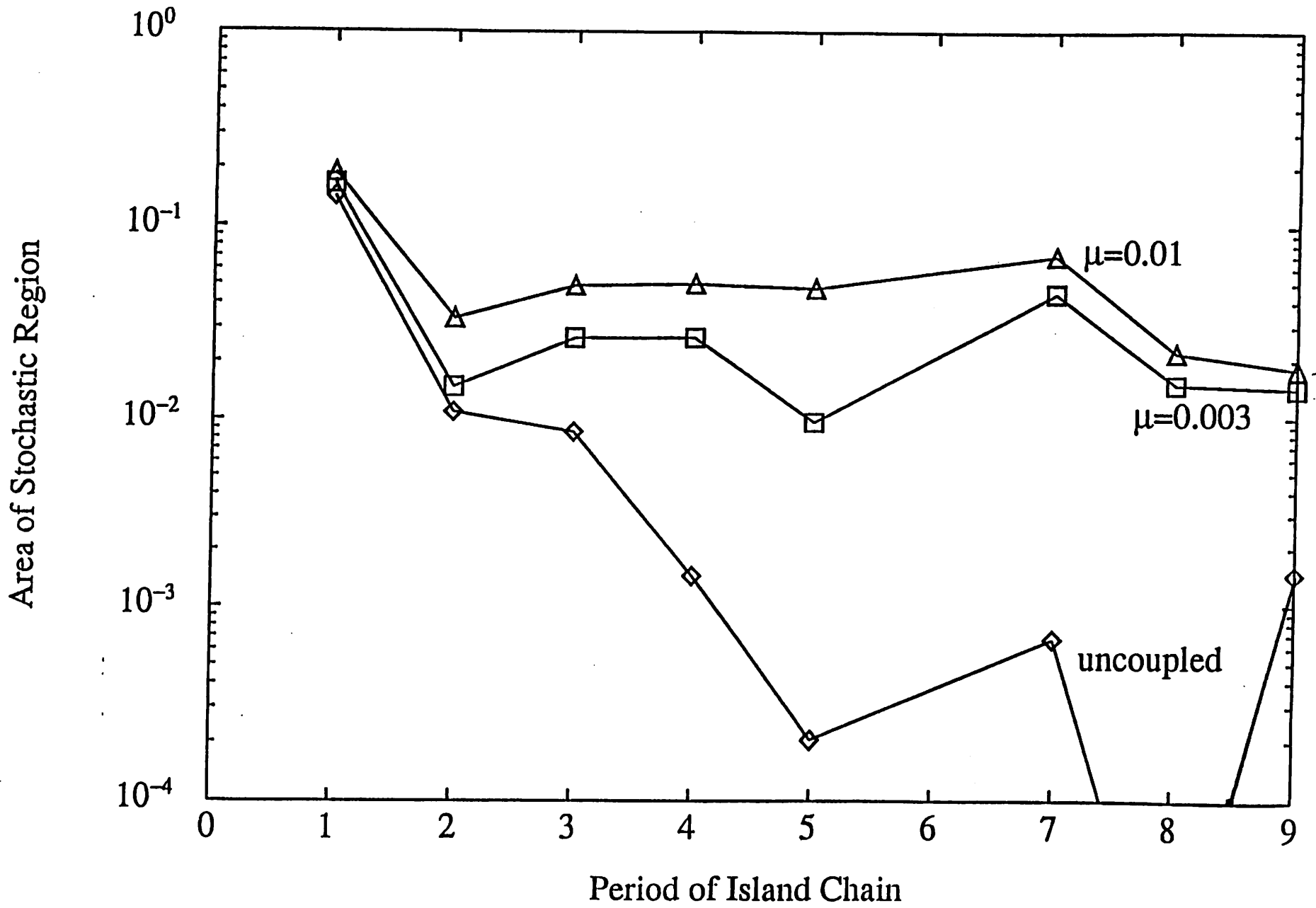


Figure 8

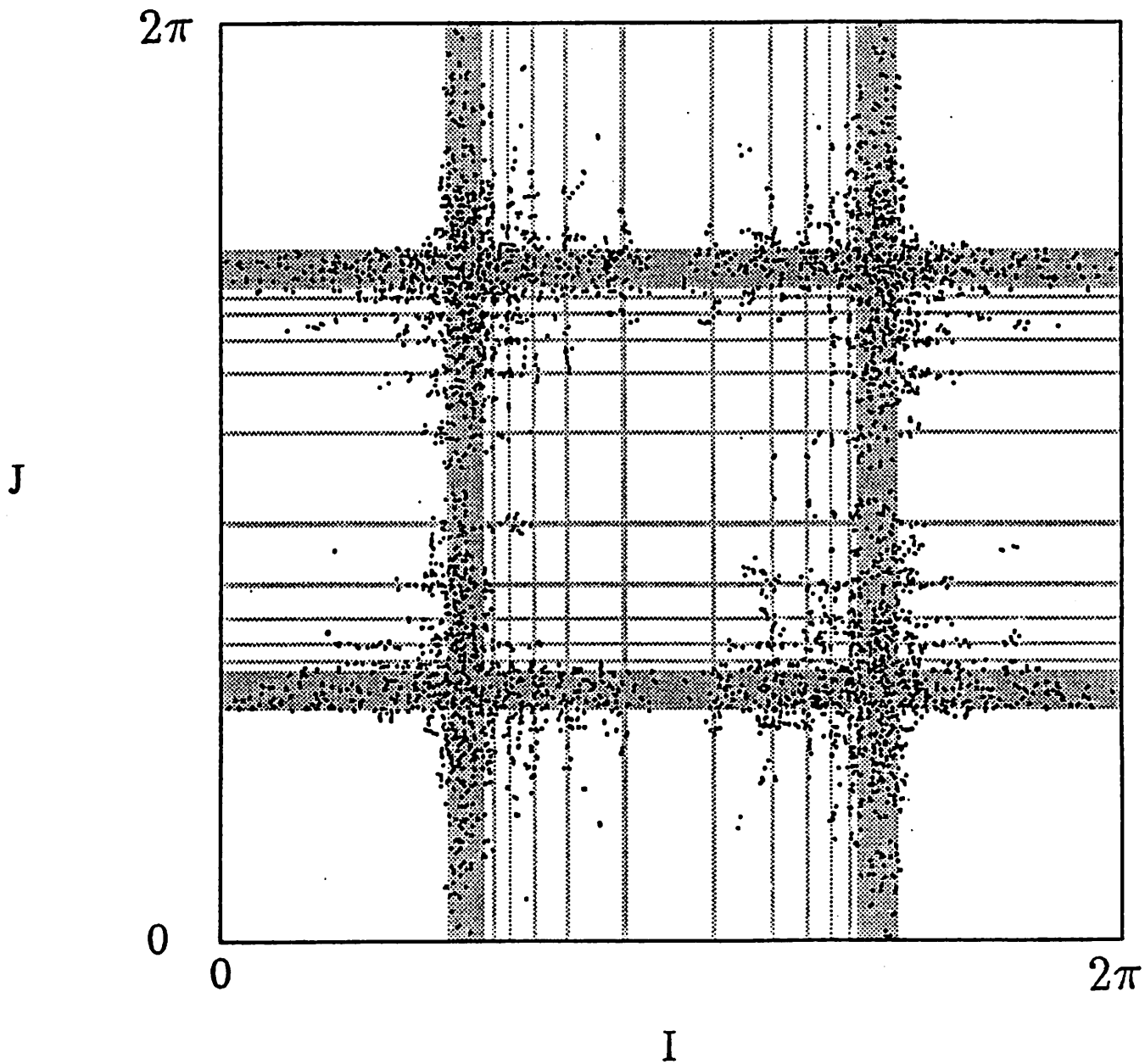


Figure 9

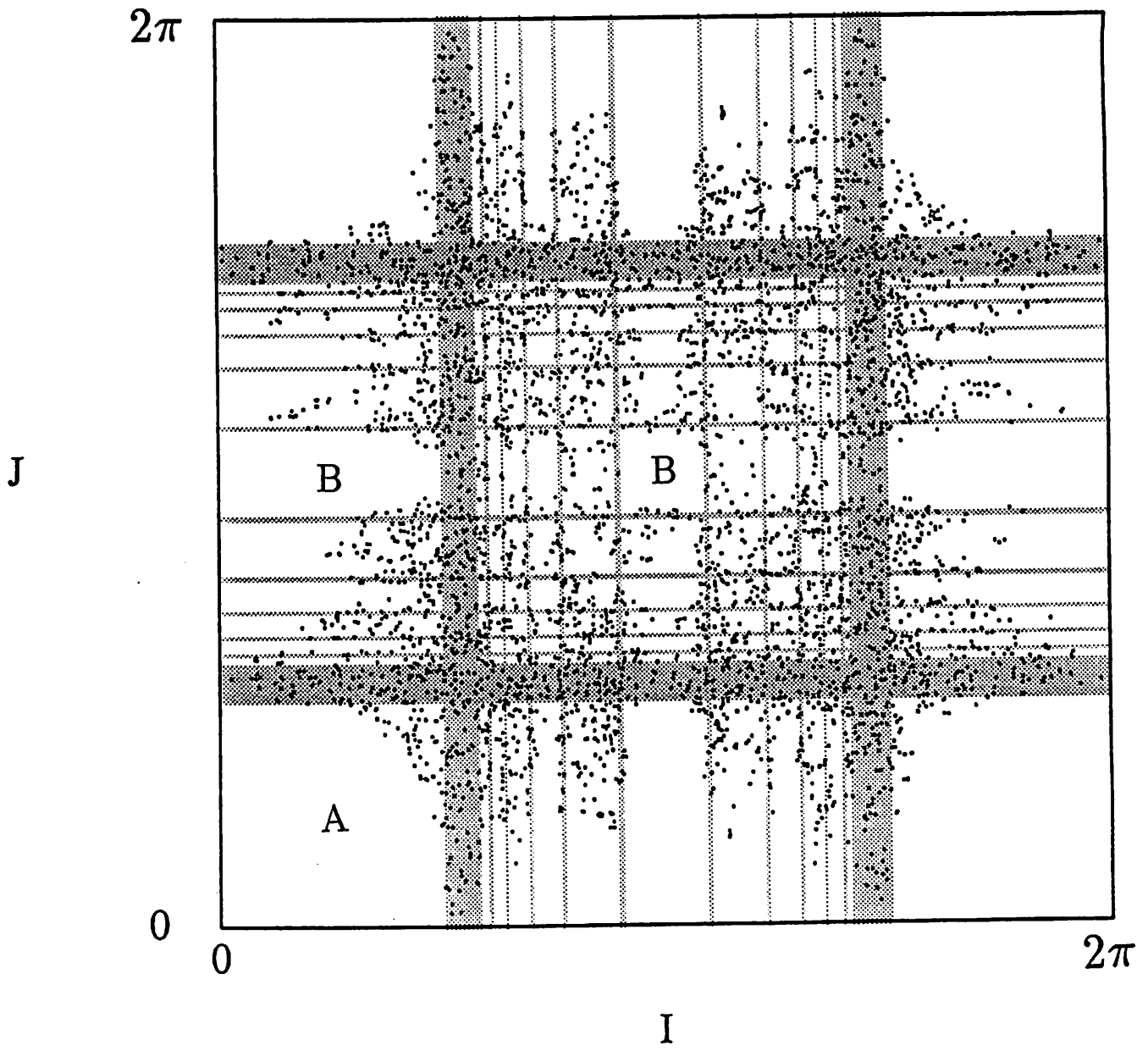


Figure 10

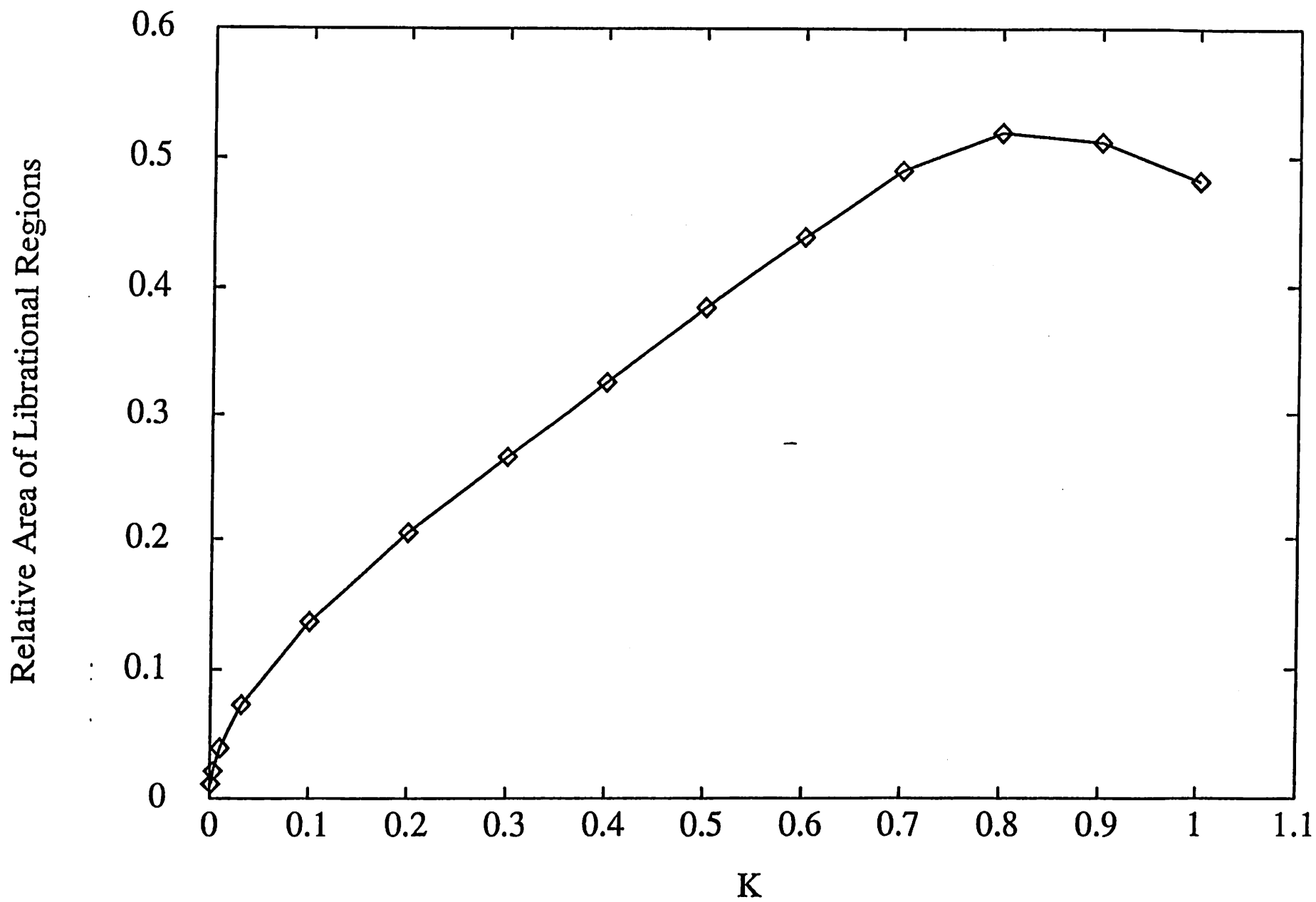


Figure 11

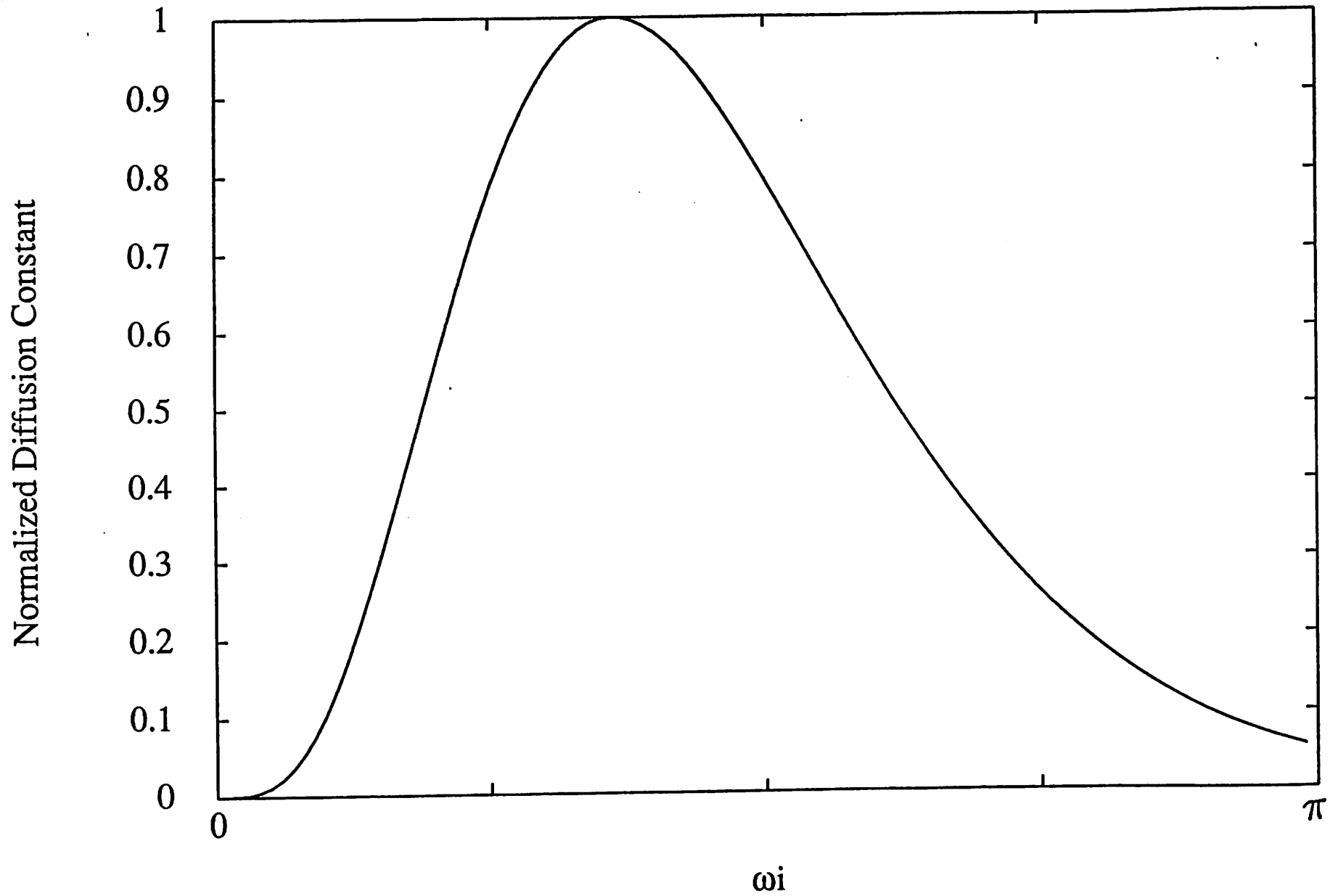


Figure 12

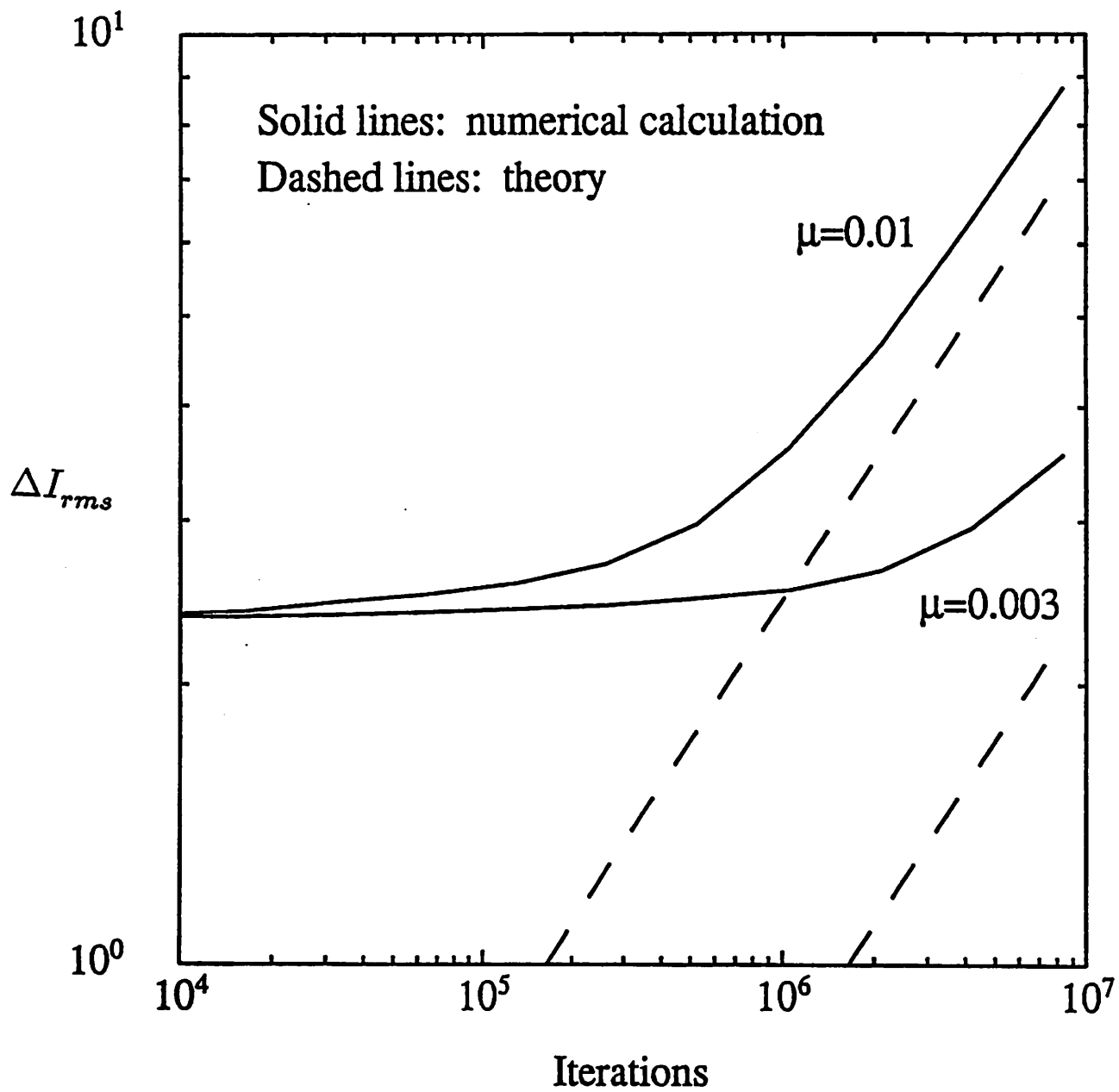


Figure 13